Chemical Engineering Science 94 (2013) 60–68

Contents lists available at SciVerse ScienceDirect

Chemical Engineering Science

journal homepage: www.elsevier.com/locate/ces

Continuous rise velocity of air bubbles in non-Newtonian biopolymer solutions

Shahram Amirnia [a], John R. de Bruyn [b], Maurice A. Bergougnou [a], Argyrios Margaritis [a,*]

[a] Department of Chemical and Biochemical Engineering, University of Western Ontario, London, ON, Canada N6A 5B9
[b] Department of Physics and Astronomy, University of Western Ontario, London, ON, Canada N6A 3K7

HIGHLIGHTS

- Free rise of air bubbles in aqueous solutions of xanthan gum and CMC was studied.
- The rheological behavior of the biopolymer solutions was characterized.
- Xanthan Gum solutions showed elastic effects characterized by relaxation time.
- No discontinuity in the rise velocity was found over the bubble size range studied.

ARTICLE INFO

Article history:
Received 21 November 2012
Received in revised form
25 January 2013
Accepted 7 February 2013
Available online 28 February 2013

Keywords:
Bubbles
Biopolymers
Rise velocity
Xanthan gum
Carboxymethylcellulose
Non-Newtonian fluids

ABSTRACT

We have studied the free rise of small air bubbles in aqueous solutions of xanthan gum and carboxymethylcellulose. The rheological behavior of the biopolymer solutions used in our experiments was thoroughly characterized. The terminal rise velocity of the bubbles was measured by imaging their motion with a high-speed video camera. The rise velocity increased as a power law in bubble volume for the smallest bubbles studied, as expected in the Stokes flow regime, but became approximately constant for larger bubbles. We observed no discontinuity in the rise velocity over the range of bubble volumes studied, from 1 μl to 4000 μl. The shape of the bubbles changed from spherical to cusped to spherical cap as the volume increased. While the smaller bubbles rose vertically through the polymer solutions, the larger bubbles rose in a spiral or zig-zag path.

1. Introduction

Bubbles rising through non-Newtonian fluids display complex behavior, much of which remains poorly understood (Kulkarni and Joshi, 2005). Examples include the presence of a negative wake behind bubbles in viscoelastic fluids, the formation of a cusp-shaped tail, and observations of a discontinuity in bubble rise velocity (Pillapakkam et al., 2007). Small bubbles are important in bioprocessing and wastewater treatment because their high interfacial area per unit volume enhances mass transfer between gas and liquid phases (Burns et al., 1997; Krishna and van Baten, 2003). The rise velocity of the bubbles can be an important parameter in the sizing of reactors and processing systems involving bubbles, and an understanding of bubble motion is important for the overall design of such systems.

This study is focused on the motion of small (1 μl to 4000 μl) air bubbles in aqueous solutions of xanthan gum and carboxymethylcellulose (CMC). These are non-Newtonian polymeric fluids which exhibit shear-thinning behavior. Studies of aerobic fermentation of xanthan gum by *Xanthomonas campestris* have demonstrated that micro-bubbles enhance the oxygen mass transfer and significantly increase the production yield (Bangalore and Bellmer, 2006). This illustrates the importance of the behaviour of small air bubbles in aqueous solutions of biopolymers, but there have been few studies of the dynamic behavior of air bubbles in such fluids (Margaritis et al., 1999; Hassan et al., 2008).

There are conflicting reports in the literature on the existence of a discontinuity in the free rise velocity of small bubbles in non-Newtonian fluids. Wild et al. (2003) cited this phenomenon as an example of the complex behavior of bubbles, and Chhabra (2007) described the discontinuity as one of the most striking effects

* Corresponding author. Tel.: +1 519 661 2146; fax: +1 519 661 4275.
E-mail address: amarg@uwo.ca (A. Margaritis).
URL: http://www.eng.ca/people/amargaritis/ (A. Margaritis).

0009-2509/$ - see front matter © 2013 Elsevier Ltd. All rights reserved.
http://dx.doi.org/10.1016/j.ces.2013.02.032

associated with bubble motion in non-Newtonian fluids. While a number of investigators have observed a discontinuity, others have not, and in some cases experiments in the same polymer solutions have given contradictory results. Furthermore, there is disagreement as to the possible mechanisms that could give rise to such a phenomenon. Astarita and Apuzzo (1965) and Leal et al. (1971) reported a jump in the rise velocity as a function of bubble volume for small bubbles in highly elastic non-Newtonian fluids. These studies were followed by several other experiments and theoretical investigations in which a jump was observed (Calderbank et al., 1970; Liu et al., 1995; Rodrigue et al., 1996; Rodrigue and De Kee, 1999, 2002; Herrera-Velarde et al., 2003; Soto et al., 2006; Pillapakkam et al., 2007; Pilz and Brenn, 2007). Several other publications on the motion of bubbles in non-Newtonian fluids, however, reported no jump in bubble rise velocity as a function of volume (De Kee et al., 1986, 1990;

Table 1
Summary of previous investigations on the rise velocity discontinuity of bubbles in non-Newtonian fluids.

Reference	Fluids and conditions	Velocity-volume discontinuity observed?	Proposed mechanism
Astarita and Apuzzo (1965)	Carbopol, CMC, ET497, and J-100	Yes, for ET 497 and J-100. No discontinuity observed for carbopol and CMC.	Jump due to a transition in boundary conditions from no-slip for small bubbles in the Stokes regime to free surface conditions for larger bubbles
Calderbank et al. (1970)	Carbon dioxide bubbles in Polyox solutions	Yes	The bubble rear undergoes a shape change at the critical bubble volume
Leal et al. (1971)	Glass spheres and air bubbles in Polyacrylamide (PAA)	Yes, for air bubbles	Evidence for the hypothesis of Astarita and Apuzzo (1965)
Liu et al. (1995)	Polyox solutons	Yes	Reduction in drag due to the appearance of a cusped tail at a critical capillary number
De Kee et al. (1986)	CMC and PAA	No	
De Kee and Chhabra (1988)	Air, N_2, and CO_2 bubbles in CMC, PAA (Separan AP30), and PAA with surfactants	No	
De Kee et al. (1990)	PAA (Separan AP30)	No	
Rodrigue et al. (1996)	CMC, Gellan gum, Polyethylene oxide, PAA with surfactants.	Yes, for PAA solutions only	Surface modification due to presence of surfactant and elastic forces
Rodrigue and De Kee (1999)	PAA with added surfactant	Yes	Interfacial instability related to elasticity and surface tension gradients
Margaritis et al. (1999)	Various polysaccharides in solution.	No	
Dewsbury et al. (1999)	Air bubbles and buoyant particles in CMC	No	
Rodrigue and De Kee (2002)	Theoretical analysis of the free-surface problem	Yes	Discontinuity in surface forces. The existence of a cusp is a necessary but not sufficient condition for the occurrence of a discontinuity
Frank et al. (2003)	PAA	No	
Herrera-Velarde et al. (2003)	PAA, no surfactant	Yes. Bubble volume at discontinuity increased with polymer concentration.	Negative flow field around the bubbles appeared above the discontinuity
Funfschilling and Li (2006)	N_2 bubbles in CMC and PAA solutions	No	
Soto et al. (2006)	Hydrophobically-modified associative polymer solutions.	Yes	Discontinuity results from a competition between elastic and surface tension forces
Kemiha et al. (2006)	PAA	No	Negative wake behind bubbles observed
Pillapakkam et al. (2007)	Direct numerical simulations to study the role of viscoelasticity.	Yes. Magnitude of the jump varied with the concentration of solution	Shape of bubbles and wake structure changes at a critical volume
Malaga and Rallison (2007)	Numerical calculations of bubble deformation	No	
Pilz and Brenn (2007)	Praestol 2500 (PAA), polyethylene oxide, and Praestol 2540.	Yes. No discontinuity observed at low concentrations.	Relaxation time in elongational flow is important
Sikorski et al. (2009).	Carbopol	No	
Vélez-Cordero et al. (2012)	Boger-type fluids	Yes	Velocity discontinuity accompanied by formation of a small cusp at the rear of bubbles

De Kee and Chhabra, 1988; Margaritis et al., 1999; Dewsbury et al., 1999; Frank et al., 2003; Funfschilling and Li, 2006; Malaga and Rallison, 2007; Sikorski et al., 2009). This phenomenon has been reviewed in the book by Chhabra and De Kee (1992), and Table 1 summarizes the results of several relevant publications. The motion of liquid drops through non-Newtonian fluids has also been studied, with similarly conflicting results. Marrucci et al. (1970) reported that the group of Astarita and Apuzzo did not encounter any discontinuities in a study of the motion of liquid drops in non-Newtonian systems, whereas a sudden transition in both the shape and velocity of liquid drops falling in non-Newtonian fluids was reported by Fararoui and Kintner (1961).

The aim of the present study is to examine the behavior of bubbles in xanthan gum solutions, and in particular to investigate the existence of a velocity discontinuity in these fluids. Similar experiments were performed using two solutions of CMC for comparison and to check the generality of our xanthan results.

2. Experiment

Xanthan gum from *X. campestris* with a molecular weight of several million was purchased from Sigma-Aldrich Canada in powder form. CMC with molecular weight between 250,000 and 700,000 was obtained from Acros Organics. All of the solutions were made by slowly adding weighed quantities of the polymers to distilled water at 22.5 °C in a continuously-stirred 10 l tank. Stirring was continued until all of the powder was dissolved. Since a jump in bubble rise velocity has been reported in systems without surfactants (Pilz and Brenn, 2007; Herrera-Velarde et al., 2003), no surfactants were used in the experiments reported here. Seven different concentrations of xanthan gum and two concentrations of CMC were used in our experiments, as listed in Table 2. The CMC solutions were completely transparent. The xanthan solutions became more opaque as the concentration increased, making visualization experiments impossible for xanthan concentrations higher than 2580 ppm.

Experiments were performed in a transparent acrylic column similar to that used by Dewsbury et al. (1999). The column was rectangular in cross-section and measured 27 cm by 30 cm by 240 cm tall. The horizontal dimensions of the column were large compared to the size of the bubbles to minimize wall effects, and the motion of the bubbles was studied far from the ends of the column. After preparation, each solution was pumped slowly into the bubble column from the bottom, filling the column roughly half way. Time was allowed for small bubbles created by the high-shear mixer to rise to the top of the column before starting the experiments. Experiments on each solution were preformed within 24 h of its preparation.

Two Redlake MotionScope high-speed video cameras operated at 2000 frames per second were used to monitor the motion of the bubbles. The cameras were equipped with Toyo Optics zoom lenses (focal length 12.5–75 mm, f/1.8). Preliminary experiments using both cameras mounted at different heights indicated that the bubbles had reached their terminal rise velocity by the time they had risen 50 cm above the release point. Consequently, all measurements were made with a single high-speed camera positioned at that level, looking into the column from the side. Different light sources were used depending on the transparency of the solution being studied; for the more opaque, concentrated xanthan solutions, the column was backlit with a 500 W narrow-beam white-light source. The video images were stored on a computer and later analyzed using MiDAS 2.0 image processing software. The rise velocity was determined by measuring the positions of the selected bubbles in successive video images. The software was also used to measure the size of the bubbles, as discussed below, and to track their trajectories.

We used two methods to generate bubbles of known and reproducible size. The first simply involved injecting air into the experimental column with high-accuracy gastight micro-syringes (Hamilton). A concave teflon "spoon" mounted above the injection point was used to collect multiple bubbles, which coalesced to form a single large bubble of the desired volume (Dewsbury et al., 1999). The bubble was then released by inverting the spoon. This method was used with the more concentrated xanthan solutions. In the second method, used with the more transparent solutions, air was filtered to remove any traces of oil or water and then flowed continuously at a low rate into the column through a small nozzle, producing a stream of equal-sized, small, spherical bubbles as illustrated in Fig. 1. The volume of these bubbles was determined using the image processing software described above. Several of these small bubbles were collected in the teflon spoon to form a single, larger bubble which was then released. The uncertainty in the volume of the individual bubbles was approximately $\pm 5\%$.

The densities ρ of the fluid solutions used in our experiments were measured with a constant volume pycnometer at a temperature of 22.5 °C. Their surface tensions σ were measured using a Fisher Autotensiomat surface tension analyzer with a du Nouy ring. The physical properties of the solutions are tabulated in Table 2.

The rheological properties of the solutions were measured using an ARES strain-controlled shear rheometer (TA Instruments) with a cone and plate tool. Measurements under steady shear were used to determine the viscosity μ and first normal stress difference N_1 as functions of the strain rate $\dot{\gamma}$. The viscous

Table 2
Physical properties of the xanthan gum and CMC solutions. All properties were measured at 22.5 °C.

Solution	Conc. (ppm)	Density (kg/m^3)	Surface tension (mN/m)
Xanthan	520	998.5 ± 0.1	71.8 ± 0.5
	780	998.6	71.9
	1050	998.7	71.7
	1280	998.8	71.8
	1530	998.9	71.5
	2100	999.1	71
	2580	999.4	70.5
CMC	4000	999.7	71.8
	6000	1000.4	71.6
Distilled water	–	997.7	72

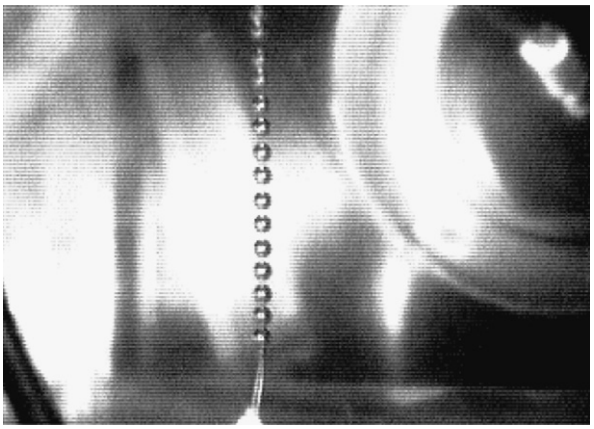

Fig. 1. A stream of equal-sized small bubbles used to create larger bubbles with known volume. The time interval between two successive bubbles was adjusted to about 10 s by a pressure regulator, and the desired number of small bubbles was combined to produce a single larger bubble.

and elastic moduli, G'' and G', respectively, were measured under small amplitude oscillatory shear at a strain amplitude of 10%. This was verified to be in the linear viscoelastic regime by measuring the moduli as a function of strain amplitude. The results of our rheological characterization are presented in Section 3.1.

3. Results and discussion

3.1. Rheological characterization

The viscosity of xanthan gum solutions with a range of concentrations are plotted in Fig. 2. Corresponding data for CMC are plotted in Fig. 3. All of the solutions studied are shear-thinning; that is, their viscosity decreases with increasing shear rate. In most cases, the viscosity at low shear rates approaches a Newtonian plateau at which its value becomes constant and independent of shear rate. This plateau is much more pronounced for the CMC solutions. For the higher concentrations of xanthan gum, the Newtonian regime is below the experimentally accessible range of shear rates. This behavior is typical of entangled polymer solutions in general. We note that there is no indication that the xanthan solutions have a yield stress.

We fit the viscosity data to a Carreau model,

$$\mu = \mu_0[1+(\lambda\dot{\gamma})^m]^{(n-1)/m}, \quad (1)$$

in which the zero-shear-rate viscosity μ_0, the relaxation time λ, and the indices n and m are fitting parameters. At low shear rates, the viscosity given by this model approaches the constant value μ_0, while at shear rates much larger than λ^{-1} the viscosity shows a power-law dependence on shear rate, behaving as $\dot{\gamma}^{n-1}$. The results are plotted in Figs. 2 and 3 for our xanthan and CMC solutions, respectively, and the fit parameters are tabulated in Table 3.

A non-zero value of N_1, the first normal stress difference, indicates the presence of elasticity. N_1 for our xanthan and CMC solutions was measured under steady shear, and is plotted as a function of $\dot{\gamma}$ in Figs. 4 and 5, respectively. We found that allowing the samples sufficient time to relax fully was essential to obtain reproducible data for N_1. The normal forces were too small to measure at the lowest shear rates, and consequently our measurements were performed for $\dot{\gamma}$ in the range 5–200 s^{-1}. Over this range of shear rates, N_1 was well described by a power law,

$$N_1 = a\dot{\gamma}^b. \quad (2)$$

Corresponding fits are plotted in Figs. 4 and 5 and the values of the parameters a and b are given in Table 4.

The elastic and viscous moduli G' and G'' for our xanthan gum solutions were measured under small-amplitude oscillatory shear and are plotted as a function of frequency in Fig. 6. The data are

Table 3
Results of fitting the viscosity data to the Carreau model, Eq. (1). The parameters are defined in the text.

Solution	Conc. (ppm)	n	m	λ (s)	μ_0 (Pa s)
Xanthan	520	0.46 ± 0.03	0.95 ± 0.12	2.6 ± 0.4	0.11 ± 0.01
	780	0.40 ± 0.03	0.70 ± 0.08	4.2 ± 0.5	0.30 ± 0.03
	1050	0.390 ± 0.009	1.00 ± 0.05	4.1 ± 0.2	0.42 ± 0.02
	1280	0.396 ± 0.008	1.17 ± 0.08	4.3 ± 0.2	0.46 ± 0.02
	1530	0.346 ± 0.005	1.00 ± 0.04	5.8 ± 0.2	0.94 ± 0.03
	2100	0.31 ± 0.02	1.0 ± 0.2	13 ± 1	2.7 ± 0.1
	2580	0.29 ± 0.01	1.0 ± 0.3	16.9 ± 0.7	4.8 ± 0.1
CMC	4000	0.71 ± 0.01	1.5 ± 0.1	0.029 ± 0.003	0.0560 ± 0.0001
	6000	0.70 ± 0.02	1.3 ± 0.1	0.054 ± 0.007	0.1240 ± 0.0003

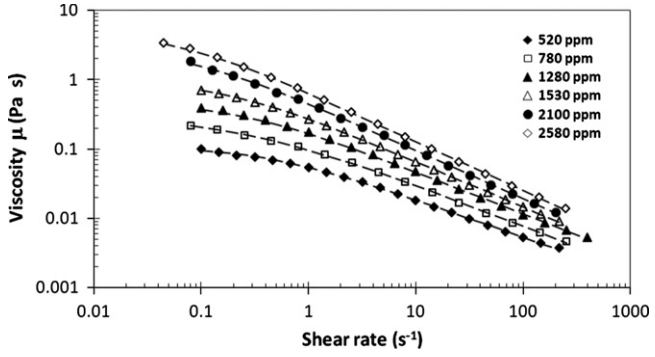

Fig. 2. Viscosity of xanthan gum solutions. The curves are fits to the Carreau model, Eq. (1).

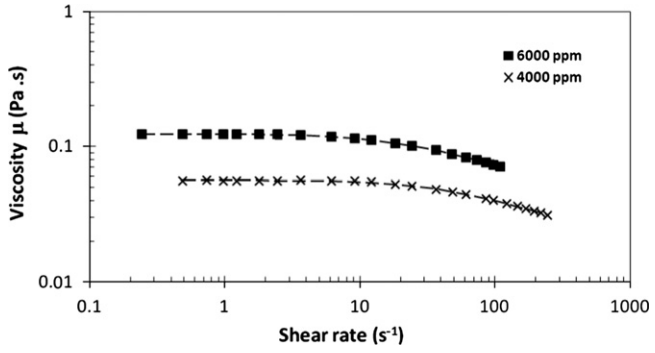

Fig. 3. Viscosity of CMC solutions. The curves are fits to Eq. (1).

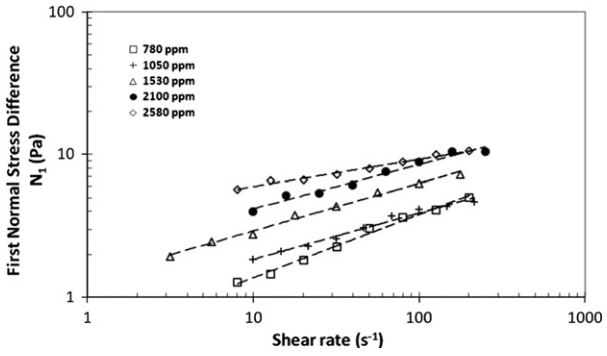

Fig. 4. First normal stress difference N1 for xanthan gum solutions. The dashed lines are fits to a power law, Eq. (2).

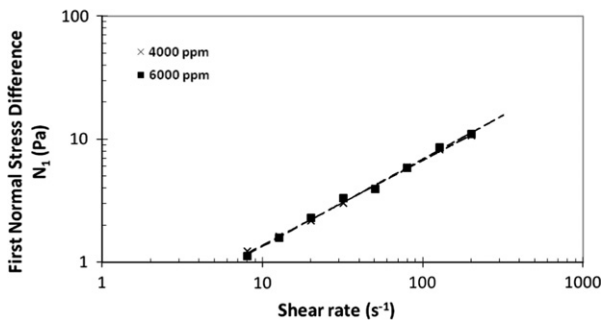

Fig. 5. First normal stress difference N1 for CMC solutions. The dashed lines are fits to a power law, Eq. (2).

Table 4
Parameters from fits of a power-law model, Eq. (2), to the first normal stress difference.

Solution	Conc. (ppm)	a (Pa s^b)	b
Xanthan	780	0.5 ± 0.08	0.44 ± 0.04
	1050	0.88 ± 0.14	0.32 ± 0.04
	1530	1.4 ± 0.8	0.33 ± 0.03
	2100	2.1 ± 0.4	0.31 ± 0.05
	2580	3.87 ± 0.14	0.19 ± 0.03
	4000	0.3 ± 0.4	0.69 ± 0.03
CMC	6000	0.26 ± 0.03	0.71 ± 0.03

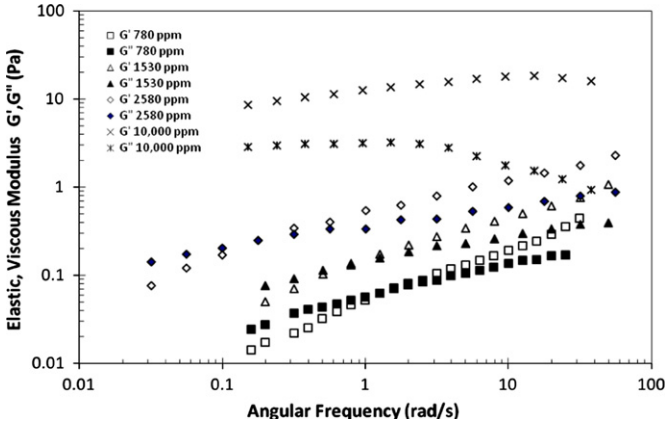

Fig. 6. Linear viscous and elastic moduli for the xanthan gum solutions.

Table 5
Crossover frequencies and relaxation times from small amplitude oscillatory shear experiments on xanthan gum and CMC solutions.

Solution	Conc. (ppm)	ω_c (rad/s)	t_c (s)
Xanthan	520	4.3 ± 0.1	1.46 ± 0.03
	780	1.3 ± 0.1	4.9 ± 0.4
	1050	0.9 ± 0.3	7 ± 2
	1280	1.0 ± 0.1	6.6 ± 0.7
	1530	0.6 ± 0.1	10 ± 2
	2100	0.31 ± 0.03	20 ± 2
	2580	0.24 ± 0.01	26 ± 1
CMC	4000	33 ± 2	0.19 ± 0.01
	6000	29 ± 2	0.21 ± 0.01

again typical of viscoelastic polymer solutions. At low frequencies, the solutions respond viscously, while at higher frequencies the elastic modulus dominates. The moduli cross over at an angular frequency ω_c, and $t_c = 2\pi/\omega_c$ is a characteristic fluid relaxation time. The crossover frequencies and the corresponding relaxation times are given in Table 5, and are consistent with the results of Milas and Rinaudo (1990). CMC displayed similar behavior but with higher crossover frequencies; the data are not plotted but are included in Table 5.

The crossover time t_c determined from the linear viscous and elastic moduli can be viewed as the longest relaxation time of the polymer molecules in the linear viscoelastic regime. On the other hand, the relaxation time λ obtained by fitting the viscosity to the Carreau equation above is measured under nonlinear (i.e., large strain) conditions. Nonetheless, the two relaxation times show consistent behavior. For xanthan gum, both time scales are on the order of a few seconds and increase approximately linearly with polymer concentration, with t_c being slightly larger than λ except at the lowest concentrations. Both time scales are much shorter for the CMC solutions, but again increase with increasing concentration. The fact that the relaxation times are much longer for the xanthan solutions indicates that they are significantly more elastic than the CMC solutions.

3.2. Bubble rise experiments

The terminal rise velocity of air bubbles in the polymer solutions of interest was measured as a function of bubble volume. We waited at least 300 s between successive bubble injections to ensure that the fluid in the experimental column was quiescent and that memory effects due to the passage of previous bubbles were negligible (Rodrigue et al., 1996).

The terminal rise velocities U measured in the xanthan gum solutions are shown in Fig. 7. For very small bubbles, the rise velocity shows a power law dependence on bubble volume. While there is some scatter between the different runs, the power law exponents in this regime are consistent with the value of 2/3 expected if the buoyant force is balanced by Stokes drag. In this regime, the rise velocity decreases as the xanthan concentration is increased, reflecting the increase in viscous drag. For larger bubbles, the rise velocity flattens out and becomes independent of both bubble volume and polymer concentration within our measurement accuracy. At low xanthan concentrations, there is some indication of a small decrease in U for intermediate-sized bubbles followed by a slight increase for the largest bubbles studied. The velocity of bubbles rising through the CMC solutions is similar, as shown in Fig. 8, and indeed approaches the same constant value at large volumes.

As discussed in the Introduction, several previous investigations have reported a discontinuous jump in the bubble rise velocity as a function of volume, while others observed no such discontinuity. As can be seen from Figs. 7 and 8, our results show no indication of a discontinuity over the range studied, which

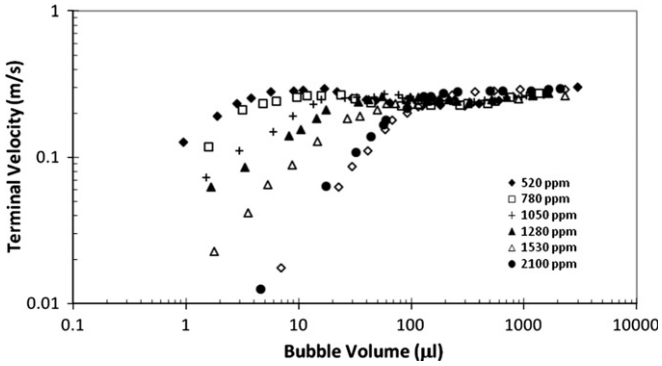

Fig. 7. Terminal rise velocity of air bubbles in aqueous solutions of xanthan gum.

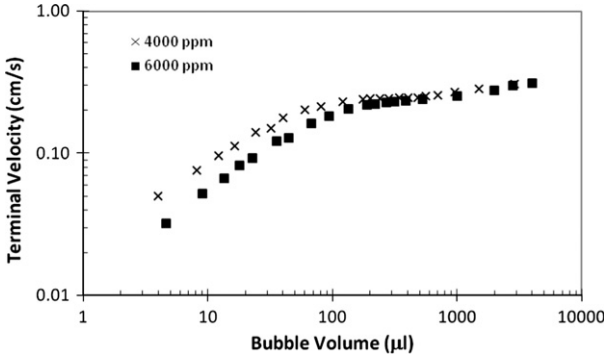

Fig. 8. Terminal rise velocity of air bubbles in aqueous solutions of CMC.

extends from well within the Stokes regime up to Reynolds numbers (as defined below) of order 100.

It has been suggested that a jump in U could result from elastic effects. Pilz and Brenn (2007) proposed a dimensionless number $\Pi = \lambda_E (g^3 \rho/\sigma)^{1/4}$, which compares the effects of elasticity and surface tension. Here g is the acceleration due to gravity and λ_E is the relaxation time in extensional flow. Pilz and Brenn (2007) argued that a velocity jump would occur when this quantity exceeded a threshold value Π_c which they found from their data to be $\Pi_c \approx 9.9$. Using the values of density and surface tension presented in Table 2 and taking account of the fact that λ_E is generally less than the relaxation time λ (Stelter et al., 2002), we find $\Pi > \Pi_c$ for all of our xanthan gum solutions, while $\Pi < \Pi_c$ for our CMC solutions. Despite this difference, we observe no velocity jump in either case, and, indeed, the functional dependence of the rise velocity on bubble volume is essentially the same for both materials. This suggests that the quantity Π is not a generally valid predictor of a velocity discontinuity.

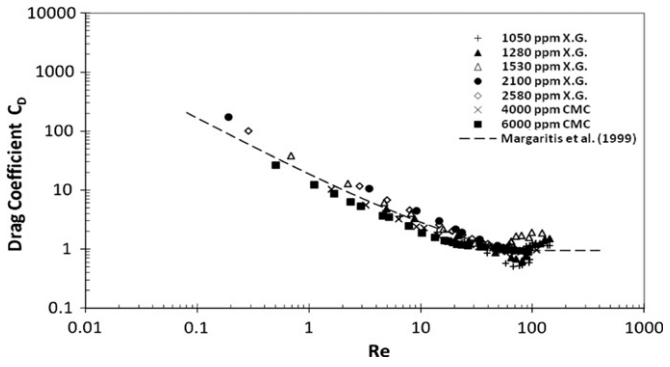

Fig. 9. The drag coefficient of the rising air bubbles plotted as a function of Reynolds number. The dashed line is the correlation obtained previously by Margaritis et al. (1999).

The drag coefficient of rising bubbles has been studied previously (Karamnev, 1994; Margaritis et al., 1999; Dewsbury et al., 1999, and Karamanev et al., 2005). The drag coefficient is defined as

$$C_D = \frac{4g\Delta\rho d_e^3}{3\rho d_h^2 U^2}, \tag{3}$$

where $\Delta\rho = \rho - \rho_{air}$ is the difference in density between the fluid and the bubbles, d_e is the equivalent diameter of the bubble (that is, the diameter of a sphere having the same volume as the bubble: $d_e^3 = 6V/\pi$ where V is the bubble volume), and d_h is the mean projected cross-sectional diameter of the bubble (which is discussed further below).

In Fig. 9 we plot C_D calculated for our bubbles as a function of the Reynolds number Re, where

$$Re = \frac{\rho U^{2-n} {d_h}^n}{k}. \tag{4}$$

The constants k and n are determined from the fits of the Carreau model to the fluid viscosity as described above, with $k = \mu_0 \lambda^{n-1}$ being the fluid consistency. In using this expression for Re, we estimated the shear rate near the bubble to be $\dot{\gamma} = U/d_h$. This is the characteristic shear rate near the equator of a spherical bubble. The effective shear rate may be slightly different for large, non-spherical bubbles, but for simplicity we use the same definition of Re in all cases. The results from all of our experiments in both xanthan gum solutions and CMC solutions collapse well onto a single curve. At low Reynolds numbers C_D decreases approximately as Re^{-1}, while the data are scattered around a value close to 1 at higher Re. Margaritis et al. (1999) studied bubbles rising through solutions of microbially-produced polysaccharides and

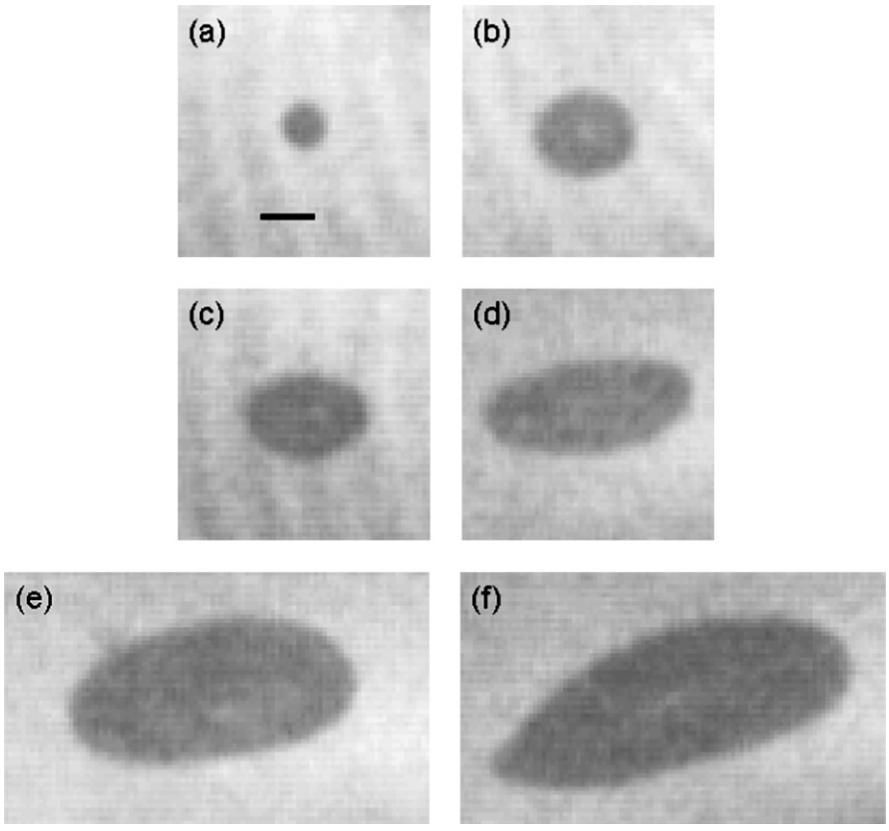

Fig. 10. Side view of air bubbles in the 1530 ppm xanthan gum solution. The image contrast is low because the xanthan solution is not fully transparent. The bubble volumes are (a) 3.5 μl; (b) 35 μl; (c) 70 μl; (d) 250 μl; (e) 550 μl; and (f) 800 μl; The scale bar shown in (a) is 0.2 cm in length.

found that their results were well described by the correlation

$$C_D = \frac{16}{Re}(1+0.173Re^{0.657}) + \frac{0.413}{1+16300Re^{-1.09}} \quad (Re < 60) \tag{5}$$

and

$$C_D = 0.95 \quad (Re \geq 60) \tag{6}$$

This correlation is also shown in Fig. 9. It describes our data well, although the value of Re at which the drag coefficient becomes constant may be slightly smaller in the present case.

The shape of the bubbles varied as a function of bubble volume. This is illustrated in Fig. 10, which shows images of several bubbles with a large range of volumes in the 1530 ppm xanthan gum solution. Fig. 11 shows images of bubbles in the 6000 ppm CMC solution. In both cases, the bubble shape changed from spherical to cusp-ended spherical to ellipsoidal and finally to spherical cap as the bubble volume increased. The largest bubbles in the CMC solutions had a more symmetric spherical cap shape than seen in bubbles in the xanthan gum solutions, but otherwise the variation in bubble shapes was similar in the two materials.

The bubble shape can be characterized using the ratio d_e/d_h of the equivalent diameter to the projected horizontal diameter (Davies and Taylor, 1950; Clift et al., 1978; Karamnev, 1994; Tzounakos et al., 2004; Margaritis et al., 1999). d_h is determined from the recorded images by taking the horizontal component of the maximum dimension of the bubble. Spherical bubbles have $d_e/d_h=1$, while d_e/d_h has been found to be 0.62 for spherical cap bubbles (Clift et al., 1978; Chhabra, 1993). As discussed further below, the values of d_h for our larger bubbles varied in time; we therefore used the time-averaged value in this analysis. In Fig. 12 we plot d_e/d_h as a function of d_e for bubbles in the 2100 ppm and 2580 ppm xanthan gum solutions. The data for these two concentrations fall on a single curve, although the same is not true for the lower concentration solutions. As expected, d_e/d_h for both biopolymers decreases from 1 for small-volume spherical bubbles to around 0.62 for the large spherical-cap shaped bubbles.

The trajectories of the bubbles also changed as their volume increased. Small, spherical bubbles traveled straight upwards, while larger bubbles followed zig-zag or spiral paths. We observed that the bubbles that rose in a straight path maintained their shape and, in particular, had a constant value of d_h as they rose. On the other

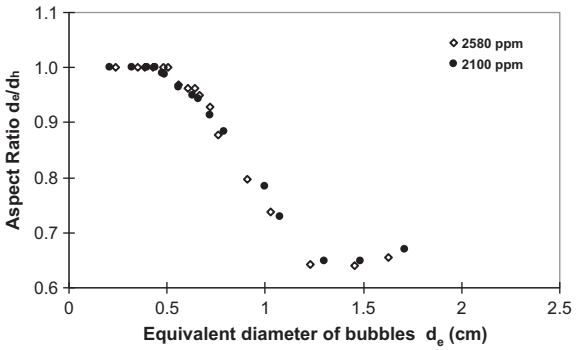

Fig. 12. Aspect ratio of air bubbles in 2100 ppm and 2580 ppm xanthan gum solutions plotted as a function of equivalent bubble diameter.

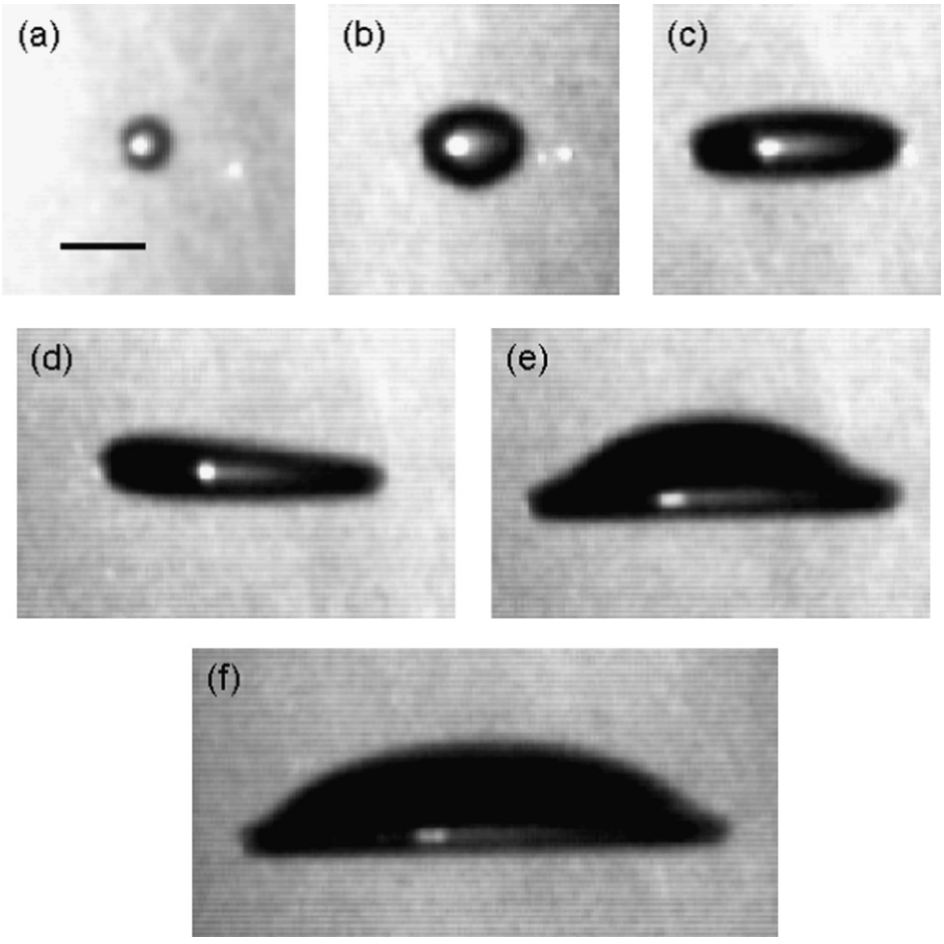

Fig. 11. Side view of air bubbles in to 6000 ppm CMC solution. The bubble volumes are (a) 18.4 μl; (b) 138 μl; (c) 553 μl; (d) 1152 μl; (e) 1844 μl; and (f) 3688 μl; The scale bar shown in (a) is 0.5 cm in length.

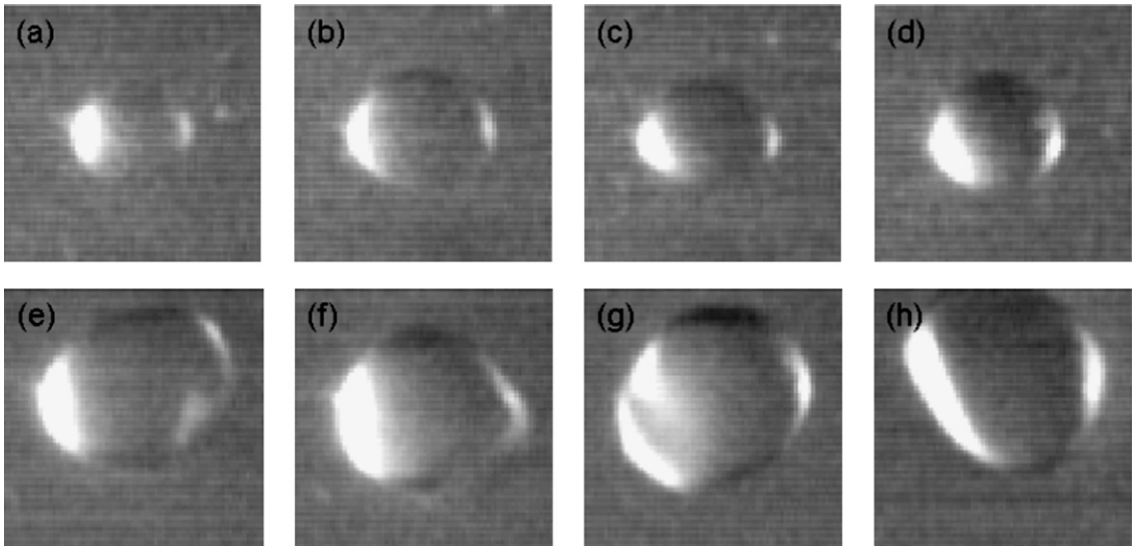

Fig. 13. (a)–(d): Top view of an 80 μl bubble rising through a 780 ppm xanthan gum solution, illustrating the changes in the bubble's cross-section with time. The bubble is approximately 0.5 cm across. Images (b)–(d) were recorded 0.067 s, 0.100 s, and 0.150 s after image (a). (e)–(h): Top view of a 300 μl bubble in the 780 ppm xanthan gum solution. The bubble is approximately 1 cm across. Images (f)–(h) were recorded 0.033 s, 0.083 s, and 0.133 s after image (e).

hand, the surfaces of bubbles that followed non-linear-trajectories deformed and their projected diameters evolved as they moved. In the case of the bubbles in the relatively concentrated xanthan gum solutions represented in Fig. 12, bubbles with $d_e/d_h > 0.7$ rose along straight, vertical paths, while those with $d_e/d_h < 0.7$ followed spiral trajectories. The change in trajectory behavior is concentration-dependent, however. Fig. 13 shows top-view images of two bubbles in a less concentrated (780 ppm) xanthan gum solution. Both of these bubbles rose along spiral trajectories. The cross-section of the bubble shown in Fig. 13(a) evolves periodically from elliptical to circular and back again. The larger bubble shown in Fig. 13(b) has a more irregular cross-section that changes continuously as it rises. The behavior of bubbles in the CMC solutions was qualitatively similar. In the analysis of the drag coefficient presented above, we used only the vertical component of the bubble velocity in Eqs. (3) and (4) to calculate *Re* and C_D for large bubbles that follow these complex trajectories.

As discussed above, a discontinuous jump in the bubble rise velocity as a function of volume has been observed in some previous experiments. In the present work, we observed no discontinuous changes in the rise velocity of our bubbles as their volume increased in either the xanthan gum solutions, which were significantly elastic, or the less-elastic CMC solutions. Indeed, the velocity-volume data for these two fluids were very similar, suggesting that elasticity does not have a large effect on the bubble motion. The rise velocity became fairly constant for our largest bubbles, and their trajectories became nonlinear. Beyond this, the substantial changes in bubble shape observed with increasing volume did not lead to any sudden changes in bubble behavior; even the appearance of a cusp-like tail on the rising bubbles did not coincide with any observable jump in the terminal velocity of the bubbles. This is consistent with the analysis of De Kee and Chan Man Fong (2002) and Pilz and Brenn (2007).

A range of physical phenomena, including surface effects due to surfactants or surface-active polymers, elastic effects at sufficiently high polymer concentrations (Rodrigue et al., 1996, 1998; Rodrigue and De Kee, 2002; Pilz and Brenn, 2007), and the appearance of a negative wake behind the bubbles (Herrera-Velarde et al., 2003) have been proposed to play a role in the occurrence of a discontinuity in the rise velocity of bubbles, but the exact cause of this phenomenon is still far from clear. The fact that a negative wake can also develop around settling solid particles without causing a discontinuity in velocity (Harlen 2002, Kemiha et al. 2006) suggests that the negative wake may be less important than surface effects or the deformability of the bubble's surface. The architecture of the polymer molecules may also play a role in any velocity discontinuity. The polymers used in the present work were rigid (xanthan) and semi-rigid (CMC) long-chain polysaccharides. In contrast, a jump in the rise velocity has most often been reported in experiments using solutions of polyacrylamide (Leal et al., 1971; Herrera-Velarde et al., 2003; Rodrigue and De Kee, 1999; Rodrigue et al., 1996), which is a flexible linear polymer.

4. Conclusions

We have studied the rise of air bubbles in surfactant-free solutions of xanthan gum and carboxymethylcellulose biopolymers. Both fluids are shear-thinning and viscoelastic, with elastic effects (characterized by the elastic relaxation time) being more important in the xanthan gum solutions. The bubbles are spherical for small volumes, but as the volume increases they develop a cusped tail, then become elliptical and, for the largest bubbles studied, have a spherical cap shape. Small bubbles rose vertically through the fluid, while larger bubbles followed spiral or zig-zag paths. The terminal rise velocity of the bubbles increased as a power law in bubble volume for small bubbles, as expected in the Stokes flow regime. For larger bubbles the rise velocity became independent of both bubble volume and the properties of the solution. No discontinuous jump in the rise velocity was observed in our experiments.

Nomenclature

V	bubble volume, μl
m, n	parameters in Carreau law, dimensionless
N_1	first normal stress difference, Pa
g	acceleration due to gravity, m/s^2
C_D	drag coefficient, dimensionless
Re	Reynolds number, dimesionless
U	terminal velocity of bubble, m/s

G'	elastic modulus, Pa
G''	viscous modulus, Pa
a, b	parameters in power-law model for normal stress difference
d	bubble diameter, cm
d_e	equivalent bubble diameter, cm
d_h	projected horizontal bubble diameter, cm
D	column diameter, cm
τ	shear stress, Pa
μ	viscosity, Pa s
$\dot{\gamma}$	shear rate, s^{-1}
μ_0	zero shear-rate viscosity, Pa s
λ	relaxation time in Equation 3.1, s
λ_E	relaxation time in elongational flow, s
ρ	density, kg/m^3
$\Delta\rho$	density difference between bubbles and surrounding fluid
σ	surface tension, mN/m

Acknowledgements

This work was supported by the Natural Science and Engineering Research Council of Canada, through Discovery Grant No.4388 awarded to Dr. A. Margaritis. We are grateful to Dr. Greg Kopp for providing the high-speed video cameras used in this work.

References

Astarita, G., Apuzzo, G., 1965. Motion of gas bubbles in non-Newtonian liquids. AlChE J. 11, 815–820.
Bangalore, D.V., Bellmer, D.D., 2006. Micro-bubbles for enhancement of oxygen transfer in xanthan gum fermentation. Chem. Eng. Commun. 193, 1232–1252.
Burns, S.E., Yiacoumi, S., Tsouris, C., 1997. Microbubble generation for environmental and industrial separation. Sep. Purif. Technol. 11, 221–232.
Calderbank, P.H., Johnson, D.S.L., Loudon, J., 1970. Mechanics and mass transfer of single bubbles in free rise through some Newtonian and non-Newtonian liquids. Chem. Eng. Sci. 25, 235–256.
Chhabra, R.P., 1993. Bubbles, Drops, and Particles in Non-Newtonian Fluids. CRC Press.
Chhabra, R.P., 2007. Bubbles, Drops, and Particles in Non-Newtonian Fluids, second ed. CRC Taylor & Francis, Chapter 6.
Chhabra, R.P., De Kee, D., 1992. Transport Processes in Bubbles, Drops, and Particles. Hemisphere Publishing Corporation, pp. 53–67.
Clift, R., Grace, J.R., Weber, M.E., 1978. Bubbles, Drops, and Particles. Academic Press, New York.
Davies, R.M., Taylor, G.I., 1950. The mechanics of large bubbles rising through extended liquids and through liquids in tubes. Proc. R. Soc. A200, 375–390.
De Kee, D., Chhabra, R.P., 1988. A photographic study of shape of bubbles and coalescence in non-Newtonian polymer solutions. Rheol. Acta 27, 656–660.
De Kee, D., Carreau, P.J., Mordarski, J., 1986. Bubble velocity and coalescence in viscoelastic liquids. Chem. Eng. Sci. 9, 2273–2283.
De Kee, D., Chhabra, R.P., Dajan, A., 1990. Motion and coalescence of gas bubbles in non-Newtonian polymer solutions. J. Non-Newtonian Fluid Mech. 37, 1–18.
De Kee, D., Chan Man Fong, C.F., 2002. Bubble shape in non-Newtonian fluid. J. Appl. Mech. 69, 703–704.
Dewsbury, K.H., Karamanev, D., Margaritis, A., 1999. Hydrodynamic characteristics of free rise of light solids and gas bubbles in non-Newtonian liquids. Chem. Eng. Sci. 54, 4825–4830.
Fararoui, A., Kintner, R.C., 1961. Flow and shape of drops in non-Newtonian fluids. Trans. Soc. Rheol. 5, 369–380.
Frank, X., Li, H.Z., Funfschilling, D., Burdin, F., Ma, Y., 2003. Bubbles motion in non-Newtonian fluids and suspensions. Can. J. Chem. Eng. 81, 483–490.
Funfschilling, D., Li, H.Z., 2006. Effects of the injection period on the rise velocity and shape of a bubble in non-Newtonian fluid. Chem. Eng. Res. Des. 84 (A10), 875–883.
Hassan, N.M.S., Khan, M.M.K., Rasul, M.G., 2008. A study of bubble trajectory and drag co-efficient in water and non-Newtonian fluids. WSEAS Trans. Fluid Mech. 3, 261–270.
Harlen, O.G., 2002. The negative wake behind a sphere sedimenting through a viscoelastic fluid. J. Non-Newtonian Fluid Mech. 108, 411–430.
Herrera-Velarde, J.R., Zenit, R., Chehata, D., Mena, B., 2003. The flow of non-Newtonian fluids around bubbles and its connection to the jump discontinuity. J. Non-Newtonian Fluid Mech. 111, 199–209.
Kemiha, M., Frank, X., Poncin, S., Li, H.Z., 2006. Origin of the negative wake behind a bubble rising in non-Newtonian fluids. Chem. Eng. Sci. 61, 4041–4047.
Karamnev, D.G., 1994. Rise of gas bubbles in quiescent liquids. AlChE J. 8, 1418–1421.
Karamanev, D., Dewsbury, K., Margaritis, A., 2005. Comments on the free rise of gas bubbles in non-Newtonian liquids: letter to the editor. Chem. Eng. Sci. 60, 4655–4657.
Kulkarni, A.A., Joshi, J.B., 2005. Bubble formation and bubble rise velocity in gas–liquid systems: a review. Ind. Eng. Chem. Res. 44, 5873–5931.
Krishna, R., van Baten, J.M., 2003. Mass transfer in bubble columns. Catalysis Today (Elsevier) 79–80, 67–75.
Leal, L.G., Skoog, J., Acrivos, A., 1971. On the motion of gas bubbles in viscoelastic liquids. Can. J. Chem. Eng. 49, 569–575.
Liu, Y.J., Liao, O.T.Y., Joseph, D.D., 1995. A two-dimensional cusp at the trailing edge of an air bubble rising in a viscoelastic liquid. J. Fluid Mech. 304, 321–342.
Malaga, C., Rallison, J.M., 2007. A rising bubble in a polymer solution. J. Non-Newtonian Fluid Mech. 141, 59–78.
Margaritis, A., teBokkel, D.W., Karamanev, D.G., 1999. Bubble rise velocities and drag coefficient in non-Newtonian polysaccharide solutions. Biotechnol. Bioeng. 64, 257–266.
Marrucci, G., Apuzzo, G., Astarita, G., 1970. Motion of liquid drops in non-Newtonian systems. AlChE J. 16, 538–541.
Milas, M., Rinaudo, M., 1990. Flow and viscoelastic properties of xanthan gum solutions. Macromolecules 23, 2506–2511.
Pillapakkam, S.B., Singh, P., Blackmore, D., Aubry, N., 2007. Transient and steady state of a rising bubble in a viscoelastic fluid. J. Fluid Mech. 589, 215–252.
Pilz, C., Brenn, G., 2007. On the critical bubble volume at the rise velocity jump discontinuity in viscoelastic liquids. J. Non-Newtonian Fluid Mech. 145, 124–138.
Rodrigue, D., De Kee, D., Chan Man Fong, C.F., 1996. An experimental study of the effect of surfactants on the free rise velocity of bubbles. J. Non-Newtonian Fluid Mech. 66, 213–232.
Rodrigue, D., De Kee, D., Chan Man Fong, C.F., 1998. Bubble velocities: further developments on the jump discontinuity. J. Non-Newtonian Fluid Mech. 79, 45–55.
Rodrigue, D., De Kee, D., 1999. Bubble velocity jump discontinuity in polyacrylamide solutions: a photographic study. Rheol. Acta 38, 177–182.
Rodrigue, D., De Kee, D., 2002. Recent developments in the bubble velocity jump discontinuity. In: De Kee, D., Chhabra, R.P. (Eds.), Transport Processes in Bubbles, Drops, and Particles, second ed. Taylor & Francis, New York, London, pp. 79–101.
Sikorski, D., Tabuteau, H., de Bruyn, J.R., 2009. Motion and shape of bubbles rising through a yield-stress fluid. J. Non-Newtonian Fluid. Mech. 159, 10–16.
Soto, E., Goujon, C., Zenit, R., Manero, O., 2006. A study of velocity discontinuity for single air bubbles rising in an associative polymer. Phys. Fluids 18 121510-12.
Stelter, M., Brenn, G., Yarin, A.L., Singh, R.P., Durst, F., 2002. Investigation of the elongational behavior of polymer solutions by means of an elongational Rheometer. J. Rheol. 46, 507–527.
Tzounakos, A., Karamanev, D., Margaritis, A., Bergougnou, M.A., 2004. Effect of the surfactant concentration on the rise of gas bubbles in power-law non-Newtonian liquids. Ind. Eng. Chem. Res. 43, 5790–5795.
Vélez-Cordero, J.R., Sámano, D., Zenit, R., 2012. Study of the properties of bubbly flows in Boger-type fluids. J. Non-Newtonian Fluid Mech. 175-176, 1–9.
Wild, G., Poncin, S., Huai-Zhi, L., Olmos, E., 2003. Some aspects of the hydrodynamics of bubble columns. Int. J. Chem. Reactor Eng.1542-6580, 1, http://dx.doi.org/10.2202/1542-6580.1095.